Atmospheric Pollution Research

www.atmospolres.com

Estimation of the effective zone of sea/land breeze in a coastal area

Rajib Pokhrel, Heekwan Lee

School of Urban and Environmental Engineering, University of Incheon, Post Box: 406-840, 12-1 Songdo-Dong, Yeonsu-Gu, Incheon, South Korea

ABSTRACT

Sea/Land breezes that are generated by mesoscale–thermally induced winds due to the different heat capacities of the land and the sea water along coastal lines, have been important issues for coastal air environments due to their significant role for the transport and diffusion of air pollution. The meso–scale modeling tool, A2C flow/A2C t&d (A2C represents Atmospheric to Computational Fluid Dynamics and t&d represents transport and diffusion) was applied to simulate the pure Sea/Land breeze mechanism. Geographic data of resolution USGS 30" were used for setting the modeling domain with a size of 248 km × 224 km and it covers both sea and land area of the west coast of Korean peninsula. Modeling period was selected in late July for typical summer conditions. Then the initial and boundary conditions were set and the modeling was carried out.

Strong land breeze was observed around 6 a.m., just before sunrise and it was neutralized between 9 a.m.–10 a.m. then the sea breeze started. The sea breeze achieved its maximum strength around 3 p.m. when the temperature difference between surface and air above 10 m was about 15 K. Subsequently, the energy of sea breeze decreased with the decrease of solar radiation with time and again reached to transition period between 8 p.m.–10 p.m. Then the vortex of breeze was generated again along the coastal line, and enlarged its buffer zone with the increase in temperature and pressure differences between the land and sea surfaces. The vortex depth of 350 m was obtained in the early morning and about 1 000 m around 3 p.m. for the modeling period. The maximum speeds of the sea and land breezes were approximately 2.5 m/s and 1.5 m/s, respectively along the coastal line. The penetration lengths of sea and land breezes were approximately 25–30 km and 15–20km, respectively. The suction lengths of sea and land breezes were about 15–20 km and 10–15 km, respectively.

Keywords:
Sea/Land breeze
Coastal air dispersion model
Penetration/suction length

Article History:
Received: 10 March 2010
Revised: 10 July 2010
Accepted: 17 July 2010

Corresponding Author:
Heekwan Lee
Tel: +82-32-835-8468
Fax: +82-32-777-8468
E-mail: airgroup@incheon.ac.kr

© Author(s) 2011. This work is distributed under the Creative Commons Attribution 3.0 License.

doi: 10.5094/APR.2011.013

1. Introduction

The world population becomes more urbanized with an ever greater proportion located in coastal environments. More than half the worldwide population lives in cities compared to 50 years ago and approximately half of the world population now lives within 50 km along the coastline (Hodges et al., 1993; Von Bodungen et al., 2001). It is essential to understand the interaction between the emissions and the coastal atmosphere, and to maintain the coastal environment for continuously increasing population (Pryor et al., 2008). Lee et al. (2004) also reported that the air quality in coastal areas is significantly affected by local meteorological conditions. Similar opinion was given by Rong (1995) where the sea breeze and mountain induced flows play important role in controlling pollution transport over the basin or in a surrounding coastal area.

Incheon city, which is located in the mid–west coast of Korean peninsula (Figure 1), has been rapidly growing compared to other areas. Reclamation of sea shore, construction of high–rise buildings for increased population, coverage of open land by cement concrete or asphalt, etc. are the major changes in Incheon area. In addition, major energy sources (power plants), airport, seaport, etc. have been in operation along the coastal line and at nearby islands which subsequently affect the local atmospheric environment (Jung et al., 2009). This change of surface roughness by urbanization blocks the air flow in highly constructed area and accelerates it in the space between the buildings (Yamada, 2004).

Incheon city frequently experiences a circulation of wind from land to sea, i.e. land breeze, and vice–versa, i.e. sea breeze, where the sea breeze was observed about 200 days in 2000 (Jeong et al., 2008). It is generated by mesoscale–thermally induced winds due to the different heat capacities of land and sea along the coastal line. This difference produces a pressure gradient between land and sea that creates the driving force of air that flows between landward and seaward (Hsu, 1988). The characteristics of sea/land (S/L) breeze depend on the geography, land use pattern, albedo, temperature/pressure gradient, inversion height etc. and the resulting air–flow affects the transport of air pollutants from sources. Bastin (2005) reported that the vertical depths of the breeze flow were less than 200 m during the night and reached to 1 000 m during the day. Fan et al. (2008) observed that the average height of atmospheric boundary layer during night time was about 200 m, while the maximal value during day time was approximately 1 200 m. Similar results were also reported by Lee et al. (2004) and Rani et al. (2010). The inversion layer was 200–300 m during the worst atmospheric condition while the average inversion layer in Korean peninsula was about 1 000 m (Lee et al., 2004). In the same way, the properties of breeze flows also differ from one place to another, i.e. the horizontal seaward and landward extensions were about 100 km and 75 km, respectively from the sea/land interface along the west coast of Indian sub–continent (Rani et al., 2010). These results were different from those published by Jeong et al. (2008) for the west coast of Korean Peninsula. These differences in boundary layer and geography play a vital role for the dispersion of air pollutants. Fan et al. (2008), Kim et al. (2007), and Karim et al. (2007) have concluded that the winds flowing over the mountainous terrain transport the air pollutants to higher altitudes and to lower levels (plain areas). However, the horizontal penetration length at the plain areas is

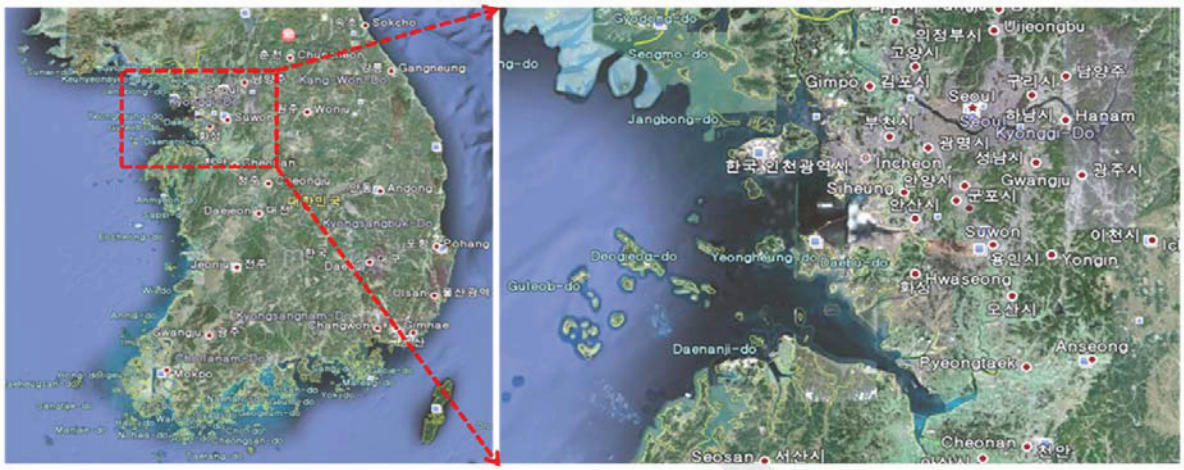

Figure 1. *Study site* ***(a)*** *Korean peninsula, and* ***(b)*** *magnification of study domain.*

longer than the mountainous areas. Together with the penetration length, the suction length plays a significant role for the transport, diffusion and settlement of pollution generated in coastal areas. Obviously, if the suction length is shorter than the penetration length, the air pollution generated and transported from coastal line by forward breeze could not return back to its origin. Hence, the mesoscale modeling technique was used in this study to understand the air dispersion mechanism and to estimate its influence zone in the study domain.

2. Atmospheric Modeling

Atmospheric systems are divided into various groups such as micro scale, mesoscale, and regional scale. Particular study cases including sea/land breeze, vegetation and snow breeze, mountain/valley wind, etc. are classified into mesoscale atmospheric systems (Pielke et al., 1994). Mesoscale atmospheric systems are sub–divided into two groups: (1) those forced primarily by surface inhomogeneities (terrain– and physiographic – induced mesoscale systems), and (2) those forced primarily by instabilities in travelling large–scale disturbances, synoptically induced mesoscale systems. First group includes sea and land breezes, mountain–valley winds, urban circulations, and forced air flow over the rough terrain; the second group includes squall lines, hurricanes, and traveling mesoscale cloud clusters (Pielke et al., 1994). This study describes the sea/land breeze mechanism in Incheon area which is classified into the first group.

2.1. Numerical S/L breeze model

Hauwritz (1947) derived the mathematical model with the assumption that the circulation takes place in vertical x–z plane, with the x–axis perpendicular to the coastline (Figure 2). Frictional force is assumed to be opposite and proportional to the wind velocity. With these assumptions, the mathematical equation of motion was derived and it was applied by Hsu (1970).

Using those equations, the average wind speed at the coastline or the penetration length of sea/land breeze can be estimated.

$$\frac{du}{dt}+ku=-\frac{1}{\rho}\left(\frac{\partial p}{\partial x}\right) \tag{1}$$

$$\frac{dw}{dt}+kw=-\frac{1}{\rho}\left(\frac{\partial p}{\partial z}\right)-g \tag{2}$$

$$C=\oint(udx+wdz)=L\bar{V} \tag{3}$$

where, u and w are the velocity components (m/s) in x and z directions, respectively, p is the pressure (N/m^2), ρ is the density (kg/m^3), g is the acceleration of gravity (m/s^2), k is a constant that represents the intensity of the frictional force, L is the length of path of integration and $\bar{V}$ is the mean speed of the sea breeze circulation along the path of integration.

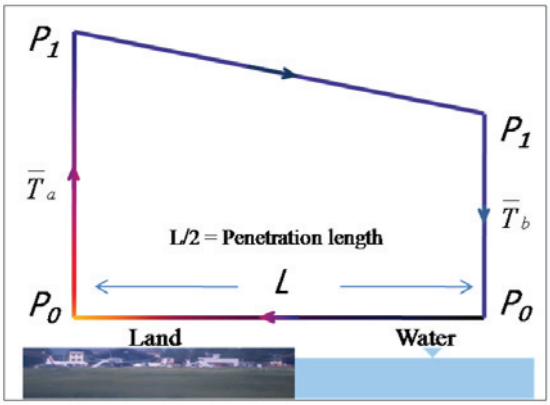

Figure 2. *Sea breeze circulation and the path of integration.*

By multiplying Equation (1) by dx, Equation (2) by dz, adding and integrating for the close path, the rate of change of circulation C is:

$$\frac{dC}{dt}=\oint\left(\frac{du}{dt}dx+\frac{dw}{dt}dz\right)=-\oint\frac{dp}{\rho}-\oint g\,dz-kC \tag{4}$$

The second integral of Equation (4) is zero because it is the closed line integral of an exact differential, assuming g to be a single-valued function of z, density ρ is the function of pressure (p) and temperature (T) hence becomes $\rho=p/RT$. From the chosen part of integration, Equation (4) can be written as:

$$\frac{dC}{dt}=R(\bar{T}_a-\bar{T}_b)\ln(p_0/p_1)-kC \tag{5}$$

From Equation (3) and Equation (5), we can get:

$$\frac{d\bar{V}}{dt}+k\bar{V}=(\bar{T}_a-\bar{T}_b)\frac{R}{L}\ln\frac{p_0}{p_1}=M(\bar{T}_a-\bar{T}_b) \tag{6}$$

The quantity $M=(R/L)ln(P_0/P_1)$ is constant, since for a fixed path of integration P_0 and P_1 are constants. In the sea-breeze case, $\overline{T_a}-\overline{T_b}$ is assumed to be periodic function of time, representing the daily change of sun, as observed by Hsu (1967) so that:

$$M(\overline{T_a}-\overline{T_b})=A\cos\omega t \tag{7}$$

where, ω is the angular velocity of earth rotation (7.29×10^{-5} s^{-1}); k is the intensity of frictional force [2×10^{-5} S^{-1}, suggested by Hauwritz (1947)]; R is the gas constant (2.87×10^{6} erg/g K); L is the total length of sea breeze circulation; $\overline{V}$ is the average wind speed; T_m is the mean temperature; and g is the gravitational acceleration.

Inserting Equation (7) into Equation (6) and integrating, the solution of the resulting differential equation is:

$$\overline{V}=Ce^{-kt}+A(k^2+\omega^2)^{-1}(\omega\sin\omega t+k\cos\omega t) \tag{8}$$

Or, mean sea breeze $\overline{V}$, due to the maximum temperature difference between land (T_{land}) and the sea (T_{sea}), is:

$$\overline{V}=\left(\frac{R}{L}\right)\ln\left(\frac{p_0}{p_1}\right)(T_{land}-T_{sea})k(k^2+\varpi^2)^{-1} \tag{9}$$

After solving the Equation (9), sea breeze circulation length can be evaluated using Equation (10):

$$L=\frac{gh}{T_m\overline{V}}(T_{land}-T_{sea})k(k^2+\varpi^2)^{-1} \tag{10}$$

$$L=\frac{0.3429\times10^5 h}{T_m\overline{V}}(T_{land}-T_{sea}) \tag{11}$$

If temperature, wind speed, and monitoring elevation are known, the breeze circulation length can be estimated numerically using the Equation (11). Generally, the penetration length is assumed as the half of the circulation length. Mean breeze speed and surface temperature can be obtained from meteorological survey (ground based station), radar data, remote sensing data, etc.

2.2. Numerical simulation

Since early 1970s, computer capability has improved sufficiently to permit three–dimensional simulations. McPherson (1970) was the first to report for such calculations of the sea breeze and was followed, for instance, by the studies of Pielke (1994), Yamada et al. (1989; 1999), Kim et al. (2007) to present scientists. Recently, numerous techniques for complex mesoscale modeling have been developed and practiced for atmospheric modeling (Fast et al., 1995; Draxler and Hess, 1998). Astitha et al. (2008) used SKIRON/Eta atmospheric and dust–modeling system, RAMS atmospheric modeling system, and air quality model CAMx. Schutze et al. (2008) used computational fluid dynamics (CFD) code FLUENT 6 together with the particle model (FPM). Lin et al. (2008) used MM5 mesoscale model to study and evaluate the impact of the heat island effect on regional weather over Taiwan. MM5 was also used by Srinivas et al. (2007) to simulate S/L breeze circulation on the south east–coast of the Chennai region in India. Although those models have a wide range of applications, they have certain limitations related to data accuracy, uncertainty of meteorological predictions and emission data produced (Evans, 2002). Those models also underestimated the surface sensible heat fluxes during stable night conditions (Srinivas et al., 2007). Mizak et al. (2007) used NOAA Buoy model to estimate the air–sea transfer rates of highly soluble gases over coastal water bodies.

The present study mostly focuses on the sea/land breeze interaction in Incheon area and used three dimensional mesoscale model "Atmospheric to Computational Fluid Dynamics (A2C flow/ A2C t&d)" where the t&d stands for transport and diffusion. A2C flow/A2C t&d is the updated version of HOTMAC/RAPTAD (Yamada, 2004). Yamada (1989; 1999; 2000; 2004) described the detailed mathematics of HOTMAC/RAPTAD and tested it for different case studies.

The basic equations of HOTMAC for mean wind, temperature, mixing ratio of water vapor, and turbulence are similar to those used by Yamada (1981; 1985). It has the addition of nested grid capability and effect of shadows produced by terrain. The terrain vertical coordinate system is used in this model in order to increase the accuracy in the treatment of surface boundary conditions.

$$z^*=\overline{H}\frac{z-z_g}{H-z_g} \tag{12}$$

where z^* and z are the transformed and Cartesian vertical coordinates, respectively; z_g is the ground elevation; $\overline{H}$ is the material surface top of the model in the z^* coordinate; and H is the corresponding height in the z – coordinate. The governing equations following the coordinate transformation based on Yamada (1981) are:

$$\frac{DU}{Dt}=f(V-V_g)+g\frac{\overline{H}-z^*}{\overline{H}}\left(1-\frac{<\theta_v>}{\theta_v}\right)\frac{\partial z_g}{\partial x}+\frac{\partial}{\partial x}\left(K_x\frac{\partial U}{\partial x}\right)+\frac{\partial}{\partial y}\left(K_{xy}\frac{\partial U}{\partial y}\right)+\frac{\overline{H}}{H-z_g}\frac{\partial}{\partial z^*}(-\overline{uw}) \tag{13}$$

$$\frac{DV}{Dt}=-f(U-U_g)+g\frac{\overline{H}-z^*}{\overline{H}}\left(1-\frac{<\theta_v>}{\theta_v}\right)\frac{\partial z_g}{\partial y}+\frac{\partial}{\partial x}\left(K_{xy}\frac{\partial V}{\partial x}\right)+\frac{\partial}{\partial y}\left(K_y\frac{\partial V}{\partial y}\right)+\frac{\overline{H}}{H-z_g}\frac{\partial}{\partial z^*}(-\overline{vw}) \tag{14}$$

$$\frac{\partial U}{\partial x}+\frac{\partial V}{\partial y}+\frac{\partial W^*}{\partial z^*}-\frac{1}{H-z_g}\left(U\frac{\partial z_g}{\partial x}+V\frac{\partial z_g}{\partial y}\right)=0 \tag{15}$$

where,

$$W^*=\frac{\overline{H}}{H-z_g}W+\frac{z^*-\overline{H}}{H-z_g}\left(U\frac{\partial z_g}{\partial x}+V\frac{\partial z_g}{\partial y}\right) \tag{16}$$

and,

$$\frac{D()}{Dt}=\frac{\partial()}{\partial t}+U\frac{\partial()}{\partial x}+V\frac{\partial()}{\partial y}+W^*\frac{\partial()}{\partial z^*} \tag{17}$$

In the above expression $<>$ indicates an average over a horizontal surface. $\theta_v=((P_0/P)^{R/C_P}(1+0.61Q_v)T)$ is the virtual potential temperature; f, is the coriolis parameter; g is the acceleration of gravity; P is the pressure; P_0 is a reference pressure; C_P is the specific heat capacity of dry air at constant pressure (1.003 J/g K); R is the gas constant for dry air (0.28704 J/g K); Q_v is the mixing ratio of water vapor; U, V, W are the mean velocities in x, y, z directions, respectively; and u, v, w are the velocity fluctuations. The second term on the right–hand side of Equations (13) and (14) indicate the effect of ground slope. For simplicity, H is specified as:

$$H=\overline{H}+z_{g\max} \tag{18}$$

where, H = 5 000 m as suggested by Yamada et al., (1988) and z_{gmax} = 1 146 m is generated based on topographic data. Expressions of the horizontal eddy viscosity coefficients K_x, K_y, and K_{xy}, were taken from Yamada (1978). Similarly, the equations for the computation of geostrophic winds U_g and V_g were taken referred from Yamada (1981).

A turbulence kinetic energy equation is given by:

$$\frac{D}{Dt}\left(\frac{q^2}{2}\right)=\frac{\partial}{\partial x}\left[K_x\frac{\partial}{\partial x}\left(\frac{q^2}{2}\right)\right]+\frac{\partial}{\partial y}\left[K_y\frac{\partial}{\partial y}\left(\frac{q^2}{2}\right)\right]+\left(\frac{\overline{H}}{H-z_g}\right)^2\frac{\partial}{\partial z^*}\left[qlS_q\frac{\partial}{\partial z^*}\left(\frac{q^2}{2}\right)\right]-\frac{\overline{H}}{H-z_g}\times\left(\overline{uw}\frac{\partial U}{\partial z^*}+\overline{vw}\frac{\partial V}{\partial z^*}\right)+\beta\overline{gw\theta_v}-\frac{q^2}{B_1 l} \quad (19)$$

and the turbulence length scale l is obtained from:

$$\frac{D}{Dt}\left(q^2 l\right)=\frac{\partial}{\partial x}\left[K_x\frac{\partial}{\partial x}\left(q^2 l\right)\right]+\frac{\partial}{\partial y}\left[K_y\frac{\partial}{\partial y}\left(q^2 l\right)\right]+\left(\frac{\overline{H}}{H-z_g}\right)^2\frac{\partial}{\partial z^*}\left[qlS_q\frac{\partial}{\partial z^*}\left(q^2 l\right)\right]+lF_1\left[\frac{\overline{H}}{H-z_g}\times\left(-\overline{uw}\frac{\partial U}{\partial z^*}-\overline{vw}\frac{\partial V}{\partial z^*}\right)+\beta\overline{gw\theta_v}\right]-\frac{q^3}{B_1}\left[1+F_2\left(\frac{1}{kz}\right)^2\right] \quad (20)$$

where, $q^2=\overline{u^2}+\overline{v^2}+\overline{w^2}$ is twice the turbulence kinetic energy; $w\theta$, turbulence heat flux; θ_v, the fluctuation part of virtual potential temperature; l, master length scale; S_q, S_l, stability functions for eddy viscosity in the q^2 and the length scale equations; β, thermal expansion coefficient $(=1/\theta_v)$; R_N, long wave radiation flux, and (F1, F2, S_q, S_l, and B_1)=(1.8, 1.33, 0.2, 0.2, and 16.6), empirical constants determined from laboratory experiments (Mellor et al., 1982). The internal heat energy equation was taken from Yamada (1981) where the long–wave radiation flux $R_N/\rho C_p$ was computed according to Sasamori (1968). Similarly, turbulence fluxes in Equations (13), (14), (19), and (20) were obtained from simplified second–moment turbulence–closure equations as suggested by Yamada (1983). Further expressions for boundary conditions were reported in Yamada et al. (1988) and updates are explained in Yamada et al. (1989). Similarly, RAPTAD (Random Particle Transport and Diffusion) is a Lagrangian model that a number of puffs are released at the source and that the change with time of puff characteristics, such as the location of the center, size and age of the puff, are computed at every time step. Brief description of RAPTAD model was reported in Yamada (1985) and updates were described in detail by Yamada et al. (1988) and Yamada (1998).

3. Modeling Method

This study especially focuses on the S/L breeze mechanism in Incheon coastal area using a numerical simulation technique. A commercial software A2Cflow/A2C(t&d), an updated version of HOTMAC/RAPTAD, was used for simulation where the CFD (Computational Fluid Dynamics) capabilities were added to HOTMAC and RAPTAD. In the updated version, HOTMAC updated as A2Cflow and RAPTAD updated as A2Ct&d. A2Cflow is a three–dimensional computer code that forecasts wind, temperature, humidity, clouds, fog, and atmospheric turbulence distributions over complex surface conditions. The governing equations are the conservation equations for mass, momentum, potential temperature deviations, water vapor, and turbulence kinetic energy. The deviations of mean values were solved instead of the absolute values of potential temperature. The magnitude of the potential temperature is about 300 K, but the deviations from the large–scale values are on the order of 10 K or less (Yamada, 2000).

This study is focused on the pure breeze cases rather than the monsoon, synoptic or external wind effect and the whole study is divided into two parts such as validation and real modeling case for the study area. The validation case study was designed to check the model performance on required boundary conditions, although the model has already been validated and suggested for coastal air flow modeling by USEPA. The modeling process has four major parts such as selecting the study domain by extracting the topographic data, setting initial conditions for A2Cflow, setting source information for A2Ct&d, and presenting the simulation results. USGS 30″ resolution geographic data (about 800 m resolution at mid latitude) was used for extracting the geographic information to set up the modeling domain. The modeling domain lied between longitude 125.22 E, latitude 36.32 N to longitude 127.95 E, latitude 38.39 N which covers Incheon, Seoul and its neighboring mountainous and sea area as in Figure 1(b) and Figure 3.

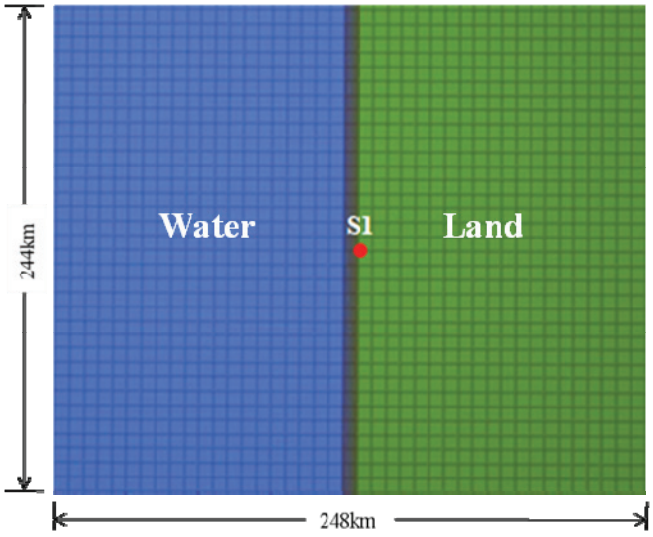

Figure 3. *Modeling domain for the validation case study.*

High temperature over 299 K in Incheon area frequently observed in late July and the average surface air temperature in July was about 297 K (Annual Climatological Report, 2008). Jeong et al. (2008) reported that the maximum number of S/L breeze days (26 days) observed on July 2006 in Incheon coastal area but there was less S/L breeze events in the east coast during the same period (NamGung et al., 2005). The average monthly air pressure at the sea level, 1 007 hPa; water vapor pressure, 25.4 hPa; relative humidity, 86%; and solar radiation intensity, 412.39 MJ/m^2 were reported in July 2008 for the study area (Annual Climatological Report, 2008).

The modeling period was selected in late July (Julian days 198–204) when the frequency of S/L breezes was at maximum. Although modeling was conducted for Julian days 198–204, results are summarized for a day (Julian day 200) which is in the middle of modeling period to avoid the effect of initial conditions. The average potential temperature, 297 K, and the reference pressure, 1 007 hPa, were setup based on references (Annual Climatological Report, 2008). The inversion height is approximately the boundary layer height during the day time in usual cases. Lee et al. (2004) and Jeong et al. (2008) reported an approximately 1 000 m inversion height during the day time in the study area. The inversion height, 1 000 m was set up as the initial condition based on the above references. Initial wind speed, 0 m/s was set by assuming the pure S/L breeze case i.e. no influence of external or synoptic wind. There was no wind flow at the beginning of modeling period and the initial wind direction is insignificant. In addition, the nudging option was set active for maintaining boundary conditions same as the initial values and HOTMAC

(A2Cflow) computations became stable. Earth rotation option set active by considering the Coriolis effect. Rest of the parameters such as turbulence variables, radiation variables, etc. was set to their default values.

Figure 3 displays the modeling domain for validation study where the size of the modeling domain was setup as same as the real modeling case. The modeling domain was designed as an ideal domain where the land surface was perfectly plain just above 1 m from the sea water surface. Except the topographical information, other initial and boundary conditions were fixed same as explained above and then the modeling was performed. Sampling point for wind flow vectors was set up about 3 km from the coastal line as in Figure 3 and 24 hour wind vector data with 1–hour intervals were used. Figure 4 presents the diurnal variation of wind speed sampled above 10 m from the surface where the negative wind speed represents the land breeze and positive wind speed represents the sea breeze. The maximum wind speed during land breeze was observed around 5 a.m., and the maximum wind speed during sea breeze was observed around 3 p.m. where the strength of sea breeze was about double of the land breeze (Figure 4). In addition, the transition periods of wind vectors were identified around 9 a.m.–10 a.m. and 8 p.m.–9 p.m. The result from this validation case agreed to the previous studies conducted by Lee et al. (2004) and Jeong et al. (2007) but the magnitude of breeze speed was different. The difference could be due to the difference in topographic data. However, the results from this case study follow the general theory of S/L breeze mechanism. In the second part, the real topographical data was considered to understand how the complex geography affects the S/L breeze mechanism in the study domain during the study period.

After the validation of the model, the real study domain was designed as in Figure 5 where the size of modeling domain, initial and boundary conditions were set using the validation case except the topographic information, grid resolution and addition of nested grids. The model domain was nested to three sub–domains (Figure 5). The sizes of the outer, interim, and inner domains were 248 km ×224 km, 200 km×168 km, and 160 km×128 km, respectively. The grid resolution of nested domain was doubled as compared to the adjacent outer domain. The grid resolutions of outer, interim and inner domains were 8 km, 4 km, and 2 km, respectively.

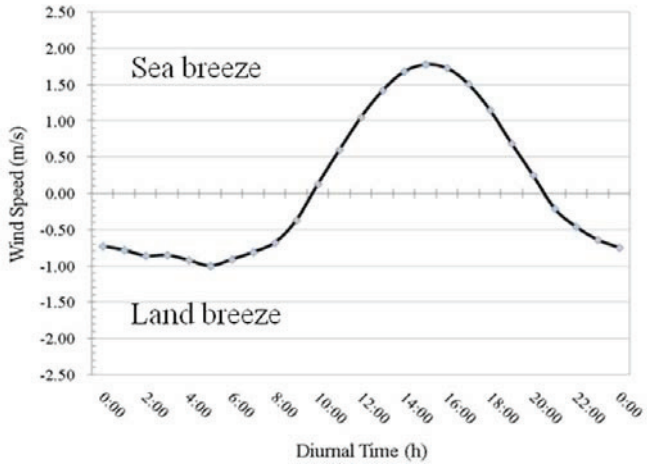

Figure 4. *Diurnal variation of wind speed at the coastal line in validation case. Negative wind speeds stand for land breeze and positive wind speeds stand for sea breeze.*

To estimate the influence zone (penetration length as well as suction length) of S/L breeze in Incheon, two different techniques were implemented. In the first case, the wind flow vectors were sampled at different locations in the study domain (Figure 5a, Table 1) and analyzed. In the second case, point sources P1–P8 were set in the study domain as in Figure 4b where puffs continuously emitted from the point sources. Point sources P1, P2, P3, and P4 were located at the landside, which were approximately 3 km, 3 km, 20 km, and 10 km, respectively away from the coastal line. The sources P5, P6, P7, and P8 were located at the seaside, which were approximately 15 km, 20 km, 35 km, and 45 km, away from the coastal line, respectively. Figures 5a and 5b show the sampling points and source points (bold lines), respectively. The puffs emitted from the point sources were diffused and transported by the breeze generated in the study domain. In this study, the most effective buffer zone of the breeze was estimated by analyzing the characteristics of wind vectors and transportation characteristics of puff by S/L breeze.

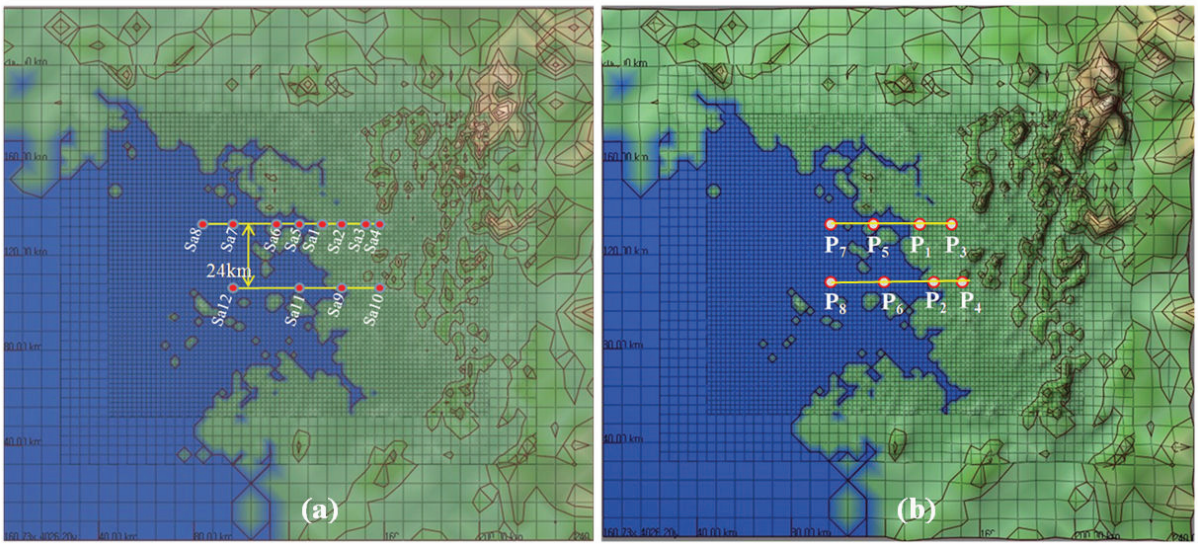

Figure 5. (a) *Sa1-Sa12 are the sampling sites of the wind vector and temperature, and* ***(b)*** *P_1-P_8 are the representation of point sources where puffs are released continuously from 65 m high and 6 m diameter stacks.*

Table 1. *Location and ground surface elevation of sampling sites in the study domain*

Sites	Surface Elevation	Remarks
Sa1	46	About 3 km far from coastal line
Sa2	9	About 10 km far from coastal line
Sa3	32	About 20 km far from coastal line and Han river is located very near to the sampling site
Sa4	39	About 25 km far from coastal line
Sa5	0	About 5 km far from coastal line and line on the sea
Sa6	5	About 15 km far from coastal line and line on the small island
Sa7	0	About 35 km far from coastal line and line on the sea
Sa8	0	About 50 km far from coastal line and line on the sea
Sa9	8	About 3 km far from coastal line
Sa10	64	About 20 km far from coastal line
Sa11	0	About 15 km far from coastal line and line on the sea
Sa12	0	About 45 km far from coastal line and line on the sea

4. Results and Discussions

After validating the mesoscale modeling software "A2C flow/A2C t&d", the domain was designed and initial conditions were set up as explained in Section 3. Wind generation in the study domain was due to the different heating capacity between sea water body and surface terrain where S/L breeze, mountain–valley breeze, and other meso–scale/micro–scale flows were generated with the diurnal variation of time. Sun radiation plays the major role for heating and cooling of the earth surface, and surface roughness controls the breeze flow by developing frictional force (Arya, 1999).

Figures 6a, 6b, 6c, and 6d display the horizontal wind vectors above 10 m from the surface level at 6 a.m., 9 a.m., 3 p.m., and 10 p.m., respectively. After the sunset, the land surface releases heat faster than the water body, subsequently the land surface temperature becomes lower than the sea water surface in late evening to early morning before sunrise. Consequently, the pressure above sea surface becomes lower than the pressure above land surface which causes the land breeze and it gains its optimal strength before sunrise (Figure 6a). The land surface heated up faster than the sea water because of the lower specific heat capacity of land surface than the water after sunshine and it reached to a neutral condition of temperature and pressure between two sides. During this transition period, neither land breeze nor sea breeze occurred (Figure 6b). As the time goes land surface heated more than the sea water that caused the temperature of the air above land surface to become higher than the sea surface. Consequently, the pressure above the land surface became lower than the pressure above the sea water surface, and then the sea breeze started to flow (Figure 6c). The transition period appeared again around 10 p.m. after the sunset (Figure 6d).

Figures 7a and 7b display the vertical cross–section of wind flow vectors at 6 a.m. when the land breeze was strong and at 3 p.m., when the sea breeze was strong. There was a visible vortex above the ground surface at about 25 km from the coastal line. The vortex and its depth help to disperse and mix the pollutants above the surface level. Vortex started from the coastal line in transition period and continuously moved toward inland with the increase of breeze strength.

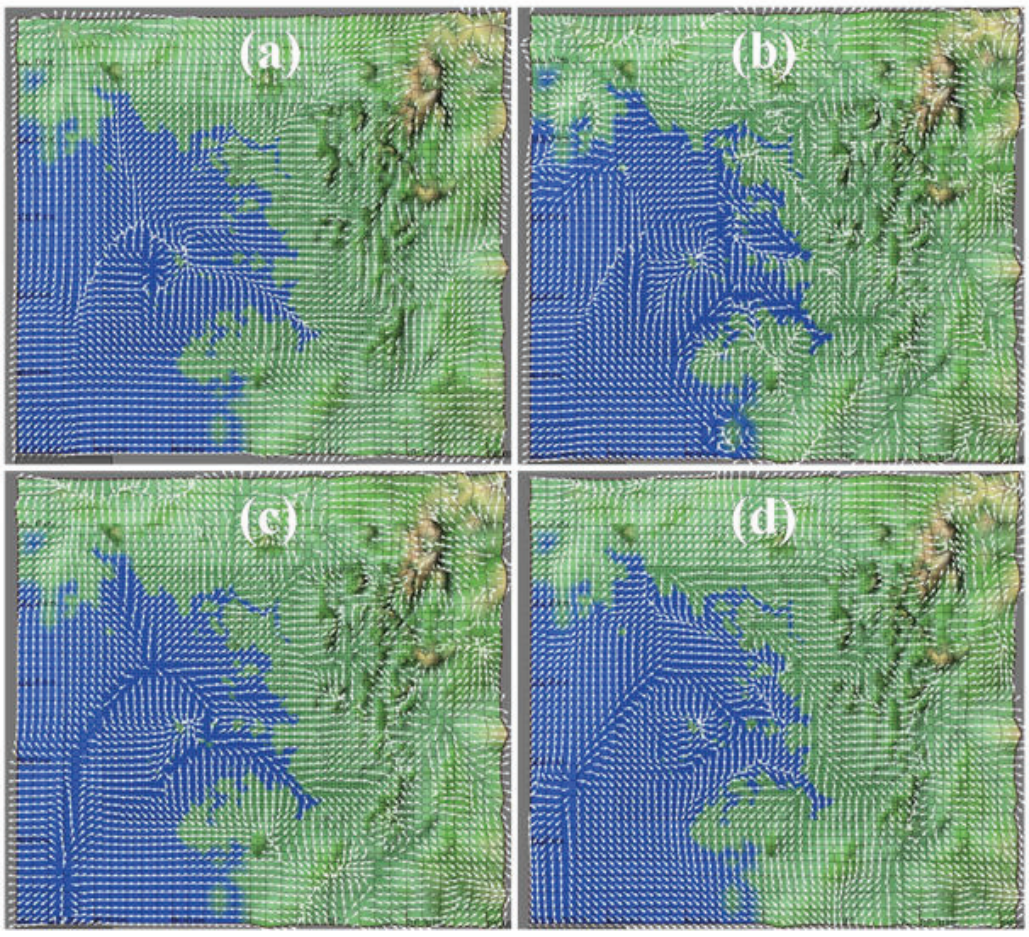

Figure 6. *Horizontal wind vector above 10 m from the surface level at* ***(a)*** *6 a.m.,* ***(b)*** *9 a.m.,* ***(c)*** *3 p.m., and* ***(d)*** *10 p.m.*

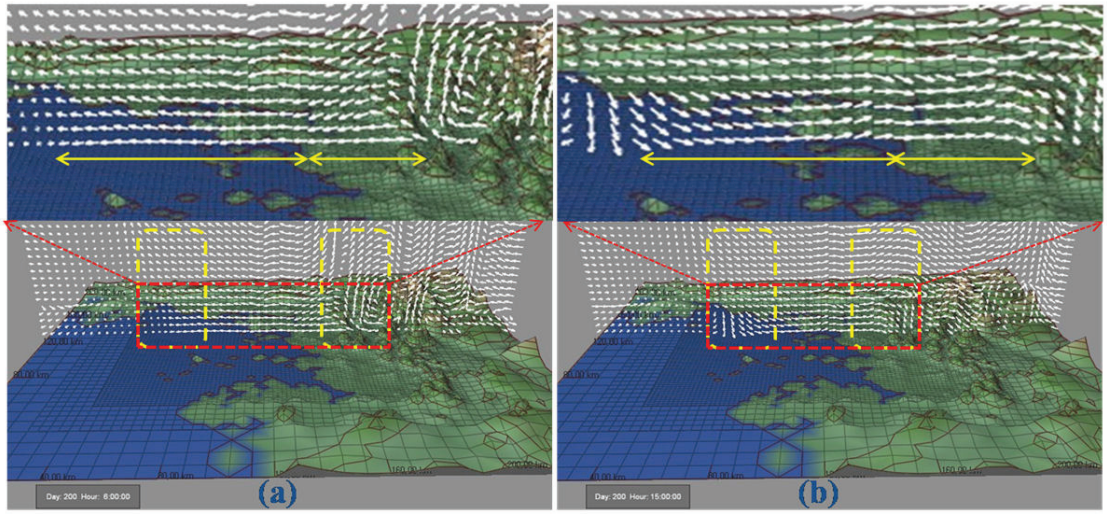

Figure 7. *Vertical wind vector at* ***(a)*** *6 a.m. - strength of land breeze was optimal and* ***(b)*** *3 p.m. – strength of sea breeze was maximum.*

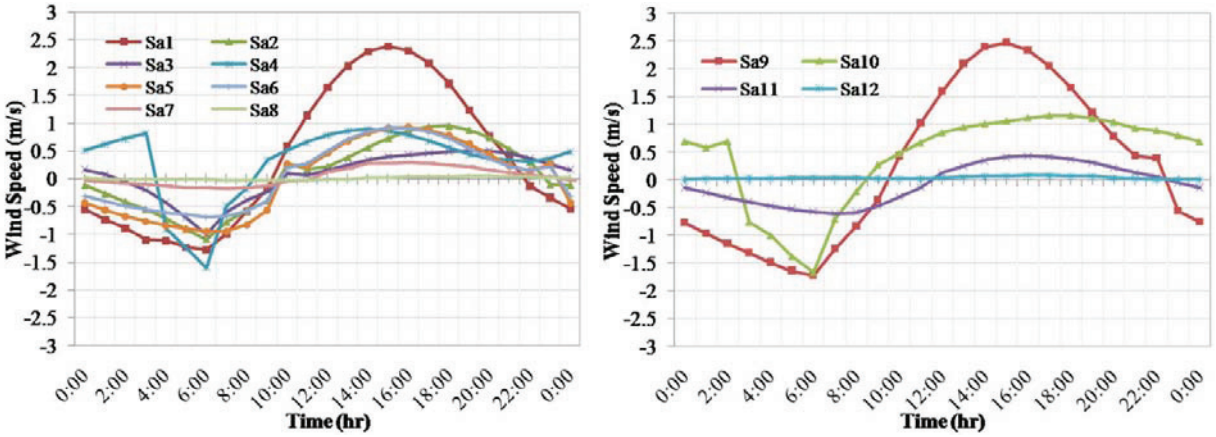

Figure 8. *Diurnal variation of wind speed above 10 m from the surface at the different sampling sites where negative wind speeds represent land breeze and positive ones represent sea breeze.*

Figures 8a and 8b display the diurnal variation of wind speed above 10 m from the surface at different sampling sites where the negative wind speeds represent the land breeze and the positive values represent the sea breeze. The geographic position of sampling sites in the modeling domain is shown in Figure 5a. Sampling sites Sa1 and Sa9 were located at about 3 km from the coastal line at inland side where the distinct land and sea breeze identified. The strength of the pure sea breeze (approximately 2.5 m/s) was about double of the land breeze. As the distance increased from the coast line, the breeze continuously lost its momentum which can be identified from the wind speed at different sampling sites in Figures 8a and 8b. There was calm wind (i.e. 0.5 m/s or less) flow at sampling sites Sa7, Sa8, and Sa12. Site Sa3 was located at 20 km from the coast line where S/L breeze lost its momentum and reached to calm condition. The result showed that the wind speed was higher at site Sa4 during the sea breeze period than Sa3, despite Sa4 was located farther than Sa3 from the coastal line. Site Sa4 is located nearby Han River (one of the major rivers of South Korea) and mountains. Mountain valley breeze frequently generated around the mountainous area (Rong et al., 1995; Bastin et al., 2005). Therefore, site Sa4 was also influenced by mountain valley breeze. Sa5, Sa6, and Sa11 were experienced pure land and sea breeze with wind speeds 0.5 m/s–1 m/s.

Figure 9 shows the diurnal variation of difference in temperature between surface and air above 10 m from the surface level. There were no noticeable differences in temperature at those sampling points located on the water surface. The maximum temperature difference of about 5 K and 15 K were observed at the sampling sites located at inland area during land breeze and sea breeze periods, respectively (Figure 9). This difference in temperature plays the major role for limiting the strength of breeze hence the strong sea breeze than the land breeze is observed.

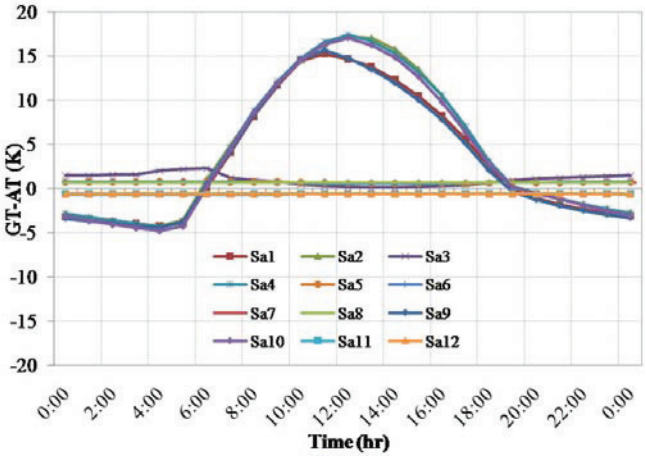

Figure 9. *Diurnal variation of temperature difference between the surface and air above 10 m Ground surface (GT) refers either to soil surface or water surface and AT refers to atmospheric temperature above 10 m from the surface.*

The major objectives of this puff dispersion modeling were to estimate the penetration and suction length of breeze, based on the distance of puffs transportation. Figure 10 displays the dispersion of pollutants from point sources shown in Figure 5b by the thermally induced breeze at the study domain at 6 a.m. (Figures 10a, 10b, 10c, 10d), 9 a.m. (Figures 10e, 10f, 10g, 10h), 3 p.m. (Figures 10i, 10j, 10k, 10l) and 10 p.m. (Figures 10m, 10n, 10o, 10p).The strength of land breeze was strong at 6 a.m. and the breeze continuously blew to seaward till the transition period started around 9 a.m. when the puffs penetrated to farthest distance. As a result, the puffs emitted near the shore line travel about 20 km to seaward. The puffs also emitted from sources P3 and P4 are dispersed to seaward during land breeze period. The source P3 is situated at about 20 km from coastal line and the puffs emitted from this source transported to seaward about 15 km from the source but did not reach to the coastal line. Source P4 is located at about 10 km away from coastal line. The puffs emitted from this source crossed the coastal line and some of them dispersed around the sea shore. According to the transportation distance of puffs by land breeze from point sources P3 and P4, the suction length of land breeze was estimated as ~15 km and the penetration length of land breeze was estimated as ~ 20 km.

The maximum speed of sea breeze was obtained around 3 p.m. and the breeze continued till late evening before starting the transition period. The puffs emitted from coast line are transported to inland area by pure sea breeze about 20 km around 3 p.m. as in Figure 10i and they continuously penetrated to inland area to late evening and dispersed up to 25–30 km from the coastal line. The local wind generated by the complex geography transports the puffs to deep inland area. Puffs reach to Sa4 and disperse near to west Seoul area and nearby mountainous area. Sources P5, P6 were located at 15 km and 20 km, respectively, where some portion of puffs emitted from P5 crossed the coastal line and dispersed to Incheon area while puffs emitted from source P6 were dispersed around the sea shore. P7 was located 35 km from coast line of mid Incheon area and it was about 15 km from northern Incheon coast area. Emissions from this source did not reach to mid Incheon coastal line but some portion dispersed to northern Incheon area (Figure 10l). In addition to this, the emissions from source P8 were dispersed around the sources that were not transported to landward by the breeze. Colors of puffs in Figure 10 vary with their age as shown. Red color represents the youngest puffs and white color represents aged puffs. Here, we focused on how far the puffs were transported by breeze. Finally, we reach to the conclusion that the penetration length and the suction length of sea breeze in this study area were 25–30 km and 15–20 km, respectively.

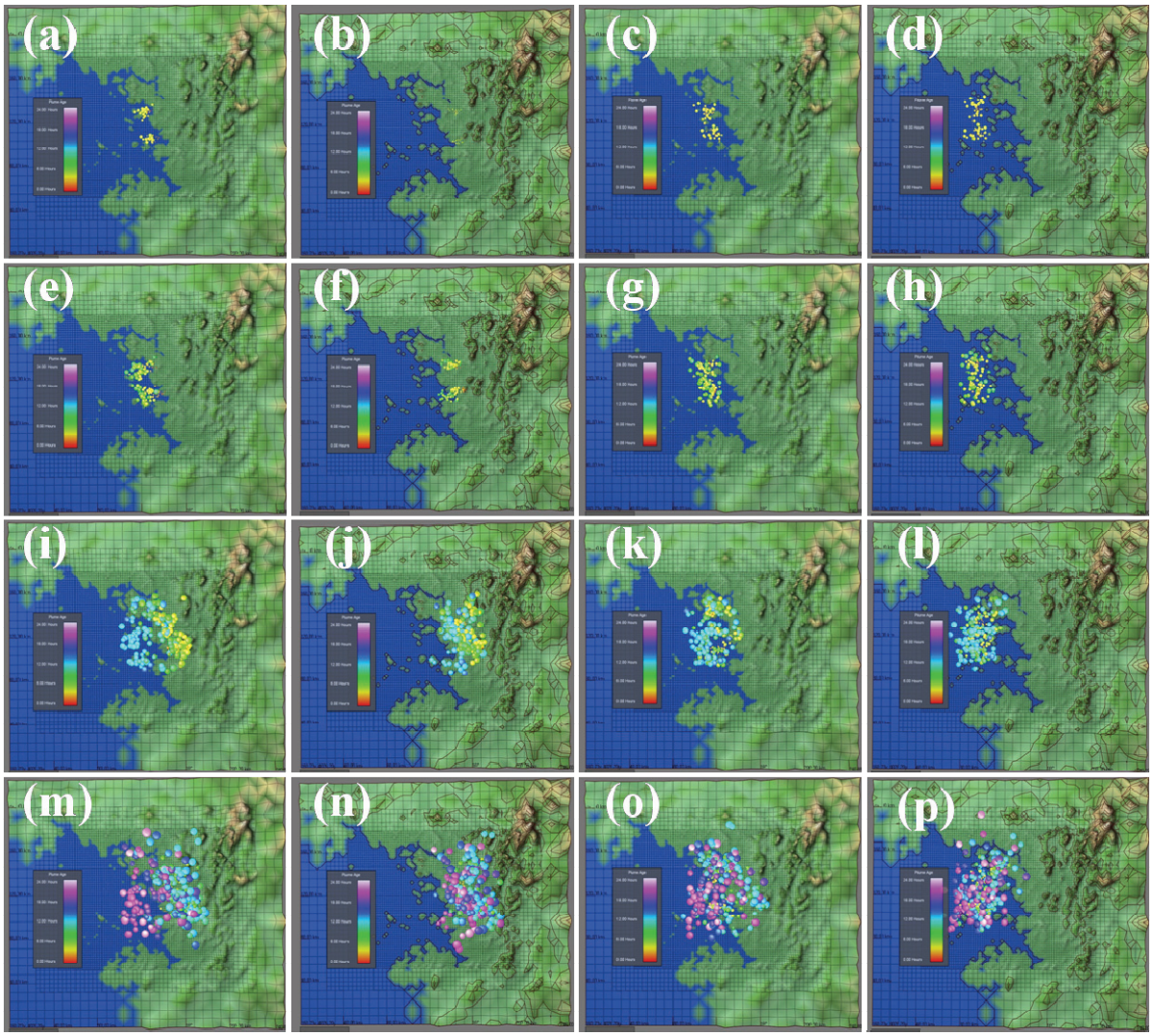

Figure 10. *Dispersion of puffs by the thermally induced breeze at the study domain from point sources at 6 a.m.* ***(a, b, c, d)****, 9 a.m.* ***(e, f, g, h)****, 3 p.m.* ***(i, j, k, l)*** *and 10 p.m.* ***(m, n, o, p)****. Columns A, B, C, and D displays the puffs emitted and dispersed at different time periods from sources (P1, P2), (P3, P4), (P5, P6), and (P7, P8), respectively.*

Meteorological parameters estimated from the modeling results are summarized in Table 2. The land surface temperature and wind velocity were taken from sampling site (Sa1) and similarly, sea surface temperature was taken from sampling site (Sa5). Approximate penetration length of sea and land breeze were also calculated by using those parameters in the analytical model shown in Equation (11). The calculated penetration length of sea breeze and land breeze were 30 km and 25 km, respectively, which were similar to the estimated penetration length from the numerical simulation.

Table 2. *Summary of wind speed and temperature variables at sampling sites (Sa1) and (Sa5)*

Parameters	Sea breeze	Land breeze
Land temperature (T_{Land})	39 °C	20 °C
Sea water temperature (T_{Sea})	25 °C	25 °C
Average temperature (T_m)	32 °C	22.5 °C
Maximum wind speed above height (h=10m)	2.5 m/s	1.5 m/s
Penetration length (L/2)	30 km	25 km

5. Conclusions

S/L breeze has been an important issue in coastal environments because of its significant role for transport and diffusion of air pollutants generated in coastal areas. In this study, meso–scale modeling tool A2C flow / A2C t&d was successfully introduced to analyze the pure S/L breeze where modeling domain of size 248 km × 224 km was set up by covering both sea and land areas of the mid–west coast of Korean Peninsula, covering Incheon area.

Strong land breeze was observed around 6 a.m. just before sunrise and it was neutralized between 9 a.m.–10 a.m. then the sea breeze started. The speed of sea breeze was maximum 3 p.m. Then the sea breeze lost its momentum as the sun radiation intensity decreased with time and then reached to transition period between 8 p.m–10 p.m. The vortex depth about 350 m obtained during strong land breeze period in the early morning and about 1 000 m during the strong sea breeze period. The maximum velocity of the pure sea breeze was approximately 2.5 m/s which was the double of land breeze at the coastal line. In the mean time, the sea breeze penetrated 25–30 km to inland area and land breeze penetrated 15–20 km to offshore, respectively. In the same way, the suction lengths of sea and land breezes were about 15–20 km and 10–15 km, respectively.

Acknowledgements

This research was a part of the project (Project no. E20829209H210000110) funded by the Ministry of Land, Transport and Maritime Affairs, Korea. We are grateful to all the researchers, especially AirGroup members for their kind support to complete this research work. We are also grateful and acknowledge the reviewers for their careful revision and invaluable suggestion regarding the paper which improved the quality of the article presented.

References

Annual Climatological Report, 2008. Korean Meteorological Administration, Seoul Korea, 2008.

Arya, S.P., 1999. *Air Pollution Meteorology and Dispersion*, Oxford University Press, Oxford, New York, pp 61-62

Astitha, M., Kallos, G., Katsafados, P., 2008. Air pollution modeling in the Mediterranean region: analysis and forecasting of episodes. *Atmospheric Research* 89, 358-364.

Bastin, S., Drobinski, P., Dabas, A., Delville, P., Reitebuch, O., Werner C., 2005. Impact of the Rhone and Durance valleys on sea-breeze circulation in the Marseille area. *Atmospheric Research* 74, 303-328.

Bouchlaghem, K., Mansour, F.B., Elouragini, S., 2007. Impact of a sea breeze event on air pollution at the Eastern Tunisian Coast. *Atmospheric Research* 86, 162-172.

Draxler, R.R., Hess, G.D., 1998. An overview of the HYSPLIT_4 modelling system for trajectories, dispersion and deposition. *Australian Meteorological Magazine* 47, 295-308.

Evans, R.W., 2002. *Quantification of the Effects of Data Denial and Limitation in MM5 İnitialization on Forecast Accuracy*, MSc Thesis, Air Force Institute of Technology, Ohio, United States, AFIT/GM/ENP/02M-03, 120 pp.

Fan, S., Wang, B., Tesche, M., Engelmann, R., Althausen, A., Liu, J., Zhu, W., Fan, Q., Li, M., Ta, N., Song, L., Leong, K., 2008. Meteorological conditions and structures of atmospheric boundary layer in October 2004 over Pearl River Delta area. *Atmospheric Environment* 42, 6174-6186.

Fast, J.D., O'Steen, B.L., Addis, R.P., 1995. Advanced atmospheric modeling for emergency response. *Journal of Applied Meteorology* 34, 626- 649.

Hauwritz, B., 1947. Comments on the sea breeze circulation. *Journal of Meteorology* 4, 1-8.

Hodges, C.N., Thompson, T.T., Riley, J.J., Glenn, E.P., 1993. Reversing the flow water and nutrients from the sea to the land. *Ambio* 22, 483-490.

Hsu, S.A., 1988. *Coastal Meteorology*, Academic press, Inc., London, pp. 141-179.

Hsu, S.A., 1970. Coastal air-circulation system: observations and empirical model. *Monthly Weather Review* 98, 487-509.

Hsu, S.A., 1967. Mesoscale Surface Temperature Characteristics of the Texas Coast Sea Breeze, Technical Report No. 6, Atmospheric Science Group, College of Engineering, University of Texas, Austin.

Jeong, J., Lee, I.H., Lee, H., 2008. Estimation of the effective region of sea/land breeze in west coast using numerical modeling. *Journal of Korean Society for Atmospheric Environment* 24, 259-270.

Jung, C.H, Pokarel, R., Lee, H.K., 2009. The impact of power plants on the environment and region – focus on Incheon area according to the 3rd electric support action plan. *Journal of Environmental Impact Assessment* 18, 195-208.

Kim, D., Stockwell W.R., 2007. An online coupled meteorological and air quality modeling study of the effect of complex terrain on the regional transport and transformation of air pollutants over the Western United States. *Atmospheric Environment* 41, 2319-2334.

Lee, I.H., Lee, H., 2004. Analysis of meteorological characteristics of sea/land breeze in western coastal region. *Journal of Korean Society of Urban Environment* 4, 63-71.

Lin, C.Y., Chen, W.C., Liu, S.C., Liou, Y.A., Liu, G.R., Lin, T.H., 2008. Numerical study of the impact of urbanization on the precipitation over Taiwan. *Atmospheric Environment* 42, 2934-2947.

McPherson, R.D., 1970. A numerical study of the effect of a coastal irregularity on the sea breeze. *Journal of Applied Meteorology* 9, 767-777.

Mellor, G.L., Yamada, T., 1982. Development of a turbulence closure model for geophysical fluid problems. *Reviews of Geophysics and Space Physics* 20, 851-875.

Mizak, C., Campbell, S., Sopkin,K., Gilbert, S., Luther, M., Poor, N., 2007. Effect of shoreline meteorological measurements on NOAA Buoy model prediction of coastal air sea-gas transfer. *Atmospheric Environment* 41, 4304-4309.

NamGung, J.Y., Yu, J.H., Kim, N.W., Choi, M.K., Ham, D.J., Kim, H.S., Jang, Y.J., Choi, E.K., 2005. The effect of inversion layer on the land and sea breeze circulation near the Gangneung. *Journal of Atmosphere KMS* 15, 229-239.

Pielke, R.A., Pearce, R.P., 1994. *Mesoscale modeling of the atmosphere*. Meteorological Monograph Series, American Meteorological Society, 25, Boston, pp 167.

Pryor, S.C., Barthelmie, R.J., Schoof, J.T., Binkowski, F.S., Delle Monache, L., Stull, R., 2008. Modeling the impact of sea-spray on particle concentrations in a coastal city. *Science of the Total Environment* 391, 132-142.

Rani, S.I., Ramachandran, R., Subrahamanyam, D.B., Alappattu, D.P., Kunhikrishnan, P.K., 2010. Characterization of sea/land breeze circulation along the west coast of Indian sub-continent during pre-monsoon season. *Atmospheric Research* 95, 367-378.

Rong, L., Richard, P.T., 1995. Air pollution transport in a coastal environment-II. Three-dimensional simulations over Los Angeles basin. *Atmospheric Environment* 29, 1499-1518.

Sasamori, T., 1968. The radiative cooling calculation for application to general circulation experiments. *Journal of Applied Meteorology* 7, 721-729.

Schutze, M., Stratmann, F., 2008. Numerical simulation of cloud droplet formation in a tank. *Computers and Geosciences* 34, 1034-1043.

Srinivas, C.V., Venkatesan, R., Singh, A.B., 2007. Sensitivity of mesoscale simulations of land-sea breeze to boundary layer turbulence parameterization. *Atmospheric Environment* 41, 2534-2548.

Von Bodungen, B., Turner, R.K. 2001. *Science and Integrated Coastal Management*. Berlin: Dahlem University Press, Germany, ISBN3934504027.

Yamada, T., 2004. Merging CFD and atmospheric modeling capabilities to simulate airflows and dispersion in urban areas. *Computational Fluid Dynamics Journal* 13, 329-341.

Yamada, T., 2000. Numerical simulations of airflows and tracer transport in the southwestern United States. *Journal of Applied Meteorology* 39, 399-411.

Yamada, T., 1999. A numerical simulation of urbanization on the local climate. *Journal of Wind Engineering and Industrial Aerodynamics* 81, 1-19.

Yamada, T., Kao, J.C.Y., Bunker, S., 1989. Airflow and air quality simulations over the western mountainous region with a four dimensional data assimilation technique. *Atmospheric Environment* 23, 539-554.

Yamada, T., Bunker, S., 1988. Development of a nested grid, second moment turbulence closure model and application to the 1982 ASCOT Brush Creek data simulation. *Journal of Applied Meteorology and Climatology* 27, 562-578.

Yamada, T., 1985. Numerical simulation of the night 2 data of the 1980 ASCOT experiments in the California Geysers area. *Archives for Meteorology, Geophysics, and Bioclimatology Series A* 34, 223-247.

Yamada, T., 1983. Simulation of nocturnal drainage flows by a q^2l turbulence closure model. *Journal of Atmospheric Sciences* 40, 91-106

Yamada, T., 1981. A numerical simulation of nocturnal drainage flow. *Journal of The Meteorological Society of Japan* 59, 108-122.

Yamada, T., 1978. *A three-dimensional, second order closure numerical model of mesoscale circulations in the lower atmosphere*, Argonne National Laboratory, ANL/RER-78-1, 67 pp.